

Model-Based Control of Travelling Wave Type Ultrasonic Motors

J. Maas*, T. Schulte, H. Grotstollen, N. Fröhleke

University of Paderborn, Institute for Power Electronics and Electrical Drives,
FB-14 LEA, Pohlweg 47-49, 33098 Paderborn, Germany.

* J. Maas was with the Institute g. a. and is now with the Department
Research and Technology - FT2/LA of Daimler-Chrysler in Frankfurt.

Abstract. This paper gives a review of research activities at the Institute for Power Electronics and Electrical Drives in Paderborn to the control of rotary travelling wave type ultrasonic motors. Based on a special designed hardware environment an advanced control scheme for inverter-fed travelling wave type ultrasonic motors is presented. After several modelling steps, including an averaged model for the controller design, a speed control scheme is implemented on a prototype drive. It is realized as an outer control loop of an underlaid voltage and travelling bending wave vector controller. The novel speed control is using an inverse contact model by a neural network, in order to compensate the nonlinear torque generation of the motor. The so equipped ultrasonic motor-drive meets requirements for applications in the field of servo-drives e.g. robotics. Since the reference values of the bending wave control are calculated from the desired torque value by the neural network, open loop control of the drive's torque is feasible, too.

1. Introduction

Piezoelectric ultrasonic motors (USMs), in particular rotary travelling wave type USMs, combine features such as high driving torque at low rotational speed, high holding torque, no electromagnetic interference and are more compact than conventional electro-mechanical geared motors. Thus, USMs have attracted considerable attention as a new type of actuator for special applications e.g. as actuator for robotics, medical devices or applications in aircrafts.

The driving principle of travelling wave type USMs is based on two orthogonal vibration modes which are excited to their single eigenfrequency by a piezoelectric ceramic in a first conversion stage. Superimposing both standing waves by proper amplitudes of the feeding voltage and a well defined temporal phase shift between them is producing a travelling bending wave in the stator, which performs elliptic motions of the stator's surface points. In a second energy conversion process the rotor, pressed against the stator by means of a disc spring, is driven by frictional forces related to the elliptic motions (Sashida, Kenjo, 1993). The electrical excitation of motor vibrations is applied by a special designed voltage-source two-phase inverter. Due to dielectric properties of the piezoceramic, characterized by a capacitance in each phase, two inductors have to be added in series. Thus, the USM becomes integral part of a resonant converter feeding the motor with sinusoidal voltages (Furuya, 1992).

Due to the complex and widely nonlinear characteristics of USMs intensive efforts of research are required for optimizing and exploiting the power performance of the new actuator. Beside several research activities in modelling and controlling USMs (e.g. (Sashida, Kenjo, 1993), (Furuya, 1992), (Hagood, McFarland, 1995), (Senjyu, 1995)), a simulation model for the total electro-mechanical system of travelling wave type USMs powered by resonant converters was derived in (Maas, Ide et al., 1995) including the case of a non perfect travelling wave. The basic characteristics of the actuator were studied by use of the model and the motor's torque generation was analysed in (Maas, Ide et al., 1996). Basing on the results an optimized vector control scheme was proposed in (Maas, Schulte et al., 1997) consisting of a cascaded voltage

and bending wave control. Couplings between the inner quantities and the nonlinearities of the friction interface are taken into account by this control scheme. It was implemented on the hardware environment which was described in (Maas, Fröhleke et al., 1995).

In (Maas, Schulte et al., June 1998) an advanced speed control implemented as an additional outer control loop was presented. The speed control loop is using an inverse contact model by a neural network (Maas, Schulte et al., July 1998) for compensation of the nonlinear torque generation of USMs.

Main results of research activities are summarized in this paper and it is concluded finally by the presentation of an 'Active Control Stick' as an interesting kind of application, which is based on open loop torque control by the neural network.

2. Hardware environment

In order to investigate the characteristic of USMs, to verify the simulation model and to examine the control concept by measurements, a flexible test set-up was realized which is depicted in Fig. 1a. It is described in detail in (Maas, Fröhleke et al., 1995). The control algorithm is implemented on two DSP-CPU's which are coupled to three digital peripheral boards. A PC serves for user communication.

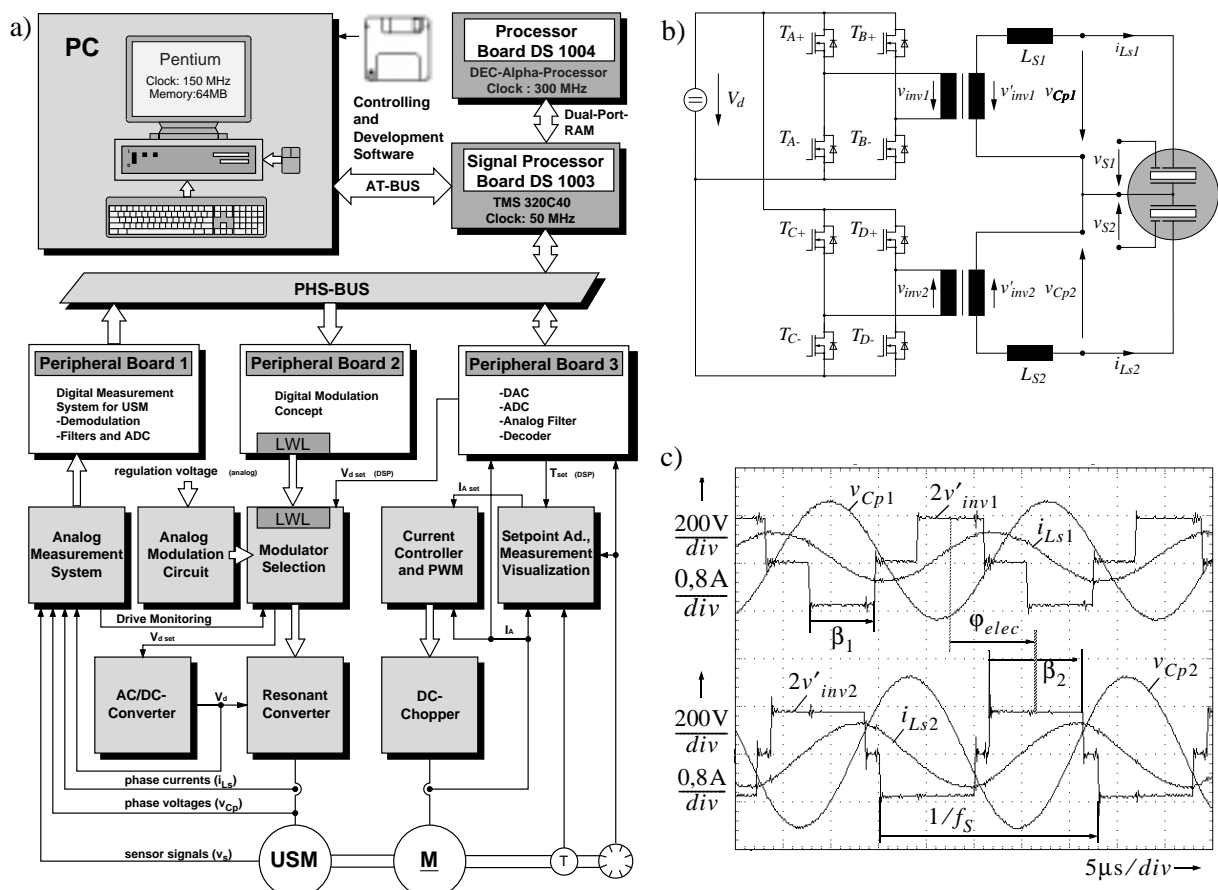


Figure 1: a) Test set-up for ultrasonic drives.

b) Two-phase resonant converter feeding USM.

c) Measured operation of two-phase resonant converter.

Peripheral board 1 contains the digital measurement system, consisting of a six channel phase sensitive demodulation system (two times motor voltages v_{cp} , currents i_{ls} and sensor signals v_s), which allows to determine the amplitude and the temporal phase shift of the measured signals. On peripheral board 2 the digital modulation concept is implemented, allowing the variation of both amplitudes, the temporal phase shift and the frequency of the motor voltages, see measurement in Fig. 1c. Thus, with respect to the control scheme all possible degrees of freedom are available for driving the converter in Fig. 1b. Peripheral board 3 contains the decoding devices of the incremental encoder and additional ADCs and DACs for further monitoring of the drive system.

The two-phase resonant converter shown at Fig. 1b consists of two full-bridge converter stages including transformers for voltage matching and insulation as well as two resonant inductors compensating the reactive power of the motor. The test set-up is completed by a current controlled DC-motor for loading the USM.

3. Modelling of USM

3.1. Model of travelling wave ultrasonic motors powered by resonant converters

USMs are characterized by a two stage energy conversion process as explained before. By the conversion processes the energy is transferred from electrical input to mechanical output terminals using different types of functional modules. Since the modules consist of electrical and mechanical components, the new actuator represents a typical example of a mechatronic system completed by a digital control for envisaged operation mode and performance. While the stage of high frequency piezoelectric energy conversion between the electrical and mechanical oscillation system can be described by linear transfer properties, the conversions stage of the micromechanical friction interface between stator and rotor displays an extreme nonlinear behaviour. Appropriate models are essential for optimization of the overall drive performance and designing the control. The simulation model derived in (Maas, Ide et al., 1995) describes the total drive system by combining the electrical as well as mechanical partial models. The signal flow diagram in Fig. 2 illustrates the overall model by which the ultrasonic oscillations of fast changing electrical state quantities $i_{Ls1,2}$, $v_{Cp1,2}$ and mechanical state quantities $\dot{w}_{1,2}$, $w_{1,2}$ are simulated. w_1 and w_2 describes the temporal amplitudes of the standing waves corresponding to both mechanical oscillation systems.

On the left hand side of Fig. 2 the resonant converter is modelled taking care of some parasitic effects like the magnetizing currents. The input block represents the inverter stage which is controlled by the quantities f_s , φ_1 , φ_2 , β_1 and β_2 as depicted at Fig. 1c. Output quantities of the converter are the motor voltages v_{Cp} , which act on the mechanical part of the USM via the inverse piezoelectric effect described by the electromechanical blocks $\hat{A}_i c_C$. The feedback of the vibrating stator on the feeding converter is given by the charges q_{mech} generated by the piezo ceramic.

The vibrating system of piezoceramic and stator is represented by a two-mode approximation (sine- and cosine-mode) considering motor unsymmetries by different modal stiffnesses $c_1 \neq c_2$ and cross-couplings by small symmetry disturbances $\varepsilon_1, \varepsilon_2$.

The interaction between mechanical subsystems is reflected by the stator/rotor-contact model describing the nonlinear mechanisms of contact forces. It is based on one hand on the model in (Flynn, 1993) in which Coulomb's friction law is postulated by neglecting tangential deformations of the contact layer. But on the other hand this model was extended in (Maas, Ide et al.,

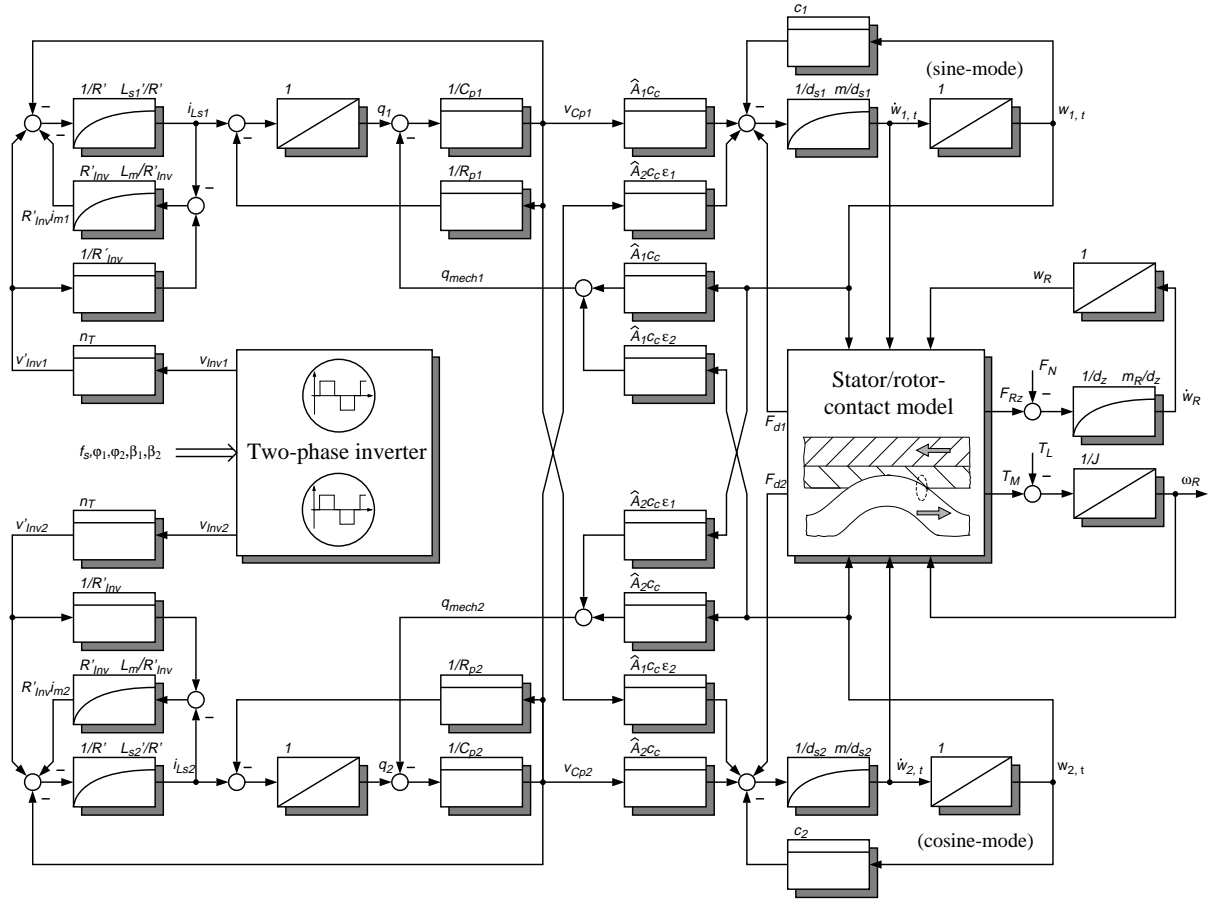


Figure 2: Signal flow diagram for the simulation model of ultrasonic drives.

1995) for the general case of a non-perfect travelling wave. Applying the general modelling approach in (Hagood, McFarland, 1995) the feedback forces F_d are taken into account additionally, which have a major impact on the stator's vibration. Contact forces acting on the rotor are given by the motor torque T_M opposing the applied load torque T_L and by the axial force F_{Rz} opposing the force F_N , which is applied by the rotor's disc spring.

In dealing with dynamics of the rotor, two degrees of freedom are taken into account. Rotor quantity ω_R models the drive's rotational speed and quantity w_R describes the axial rotor motion. While the high dynamics of the latter is less important for the control, its stationary value has a major impact on contact forces.

On one hand the simulation model reflects the high frequency ultrasonic oscillations of the electrical and mechanical resonant circuits and is therefore indispensable for detailed studies of the motor performance (Maas, Ide et al., 1995). But on the other hand the model is not suitable designing the control, because the wave shapes of the motor's voltages cannot be influenced by the inverter but only modulation of frequency, amplitude and phase is possible.

3.2. Averaged model

For obtaining an appropriate model for the control design an averaged model of the electrical and mechanical oscillation system and the friction interface is derived in (Maas, Grotstollen,

1997), which is based on the original model in Fig. 2. All variables appearing in the resonance system contain a major fundamental component shown by measurement in Fig. 1c and illustrated in several publications e.g. in (Sashida, Kenjo, 1993), (Furuya, 1992), (Senjyu, 1995). These sinusoidal waveforms can be well approximated by

$$x(t) = x_s(t) \sin(\omega t) + x_c(t) \cos(\omega t). \quad (1)$$

The averaged model reflects the slow dynamic behaviour of the oscillating original state variables $x(t)$ using their time-varying fundamental Fourier coefficients $x_s(t)$ and $x_c(t)$ (in cartesian coordinates) as new state quantities of the transformed drive model. This model, which is illustrated in Fig. 3, is predestinated for designing the control, since its controlling inputs are the fundamental voltage components

$$\mathbf{v}_{inv}^T = [v_{i1s} \ v_{i1c} \ v_{i2s} \ v_{i2c}] \quad (2)$$

of the two-phase inverter stage obtained by an appropriate vector-modulation concept for ϕ_1 , ϕ_2 , β_1 and β_2 . The electrical output quantities are given by the vector of fundamental motor voltages

$$\mathbf{v}^T = [v_{1s} \ v_{1c} \ v_{2s} \ v_{2c}] = [\mathbf{v}_1 \ \mathbf{v}_2], \quad (3)$$

exciting the mechanical subsystem of the stator by acceleration vector \mathbf{a} . The influence of the vibrating stator on the feeding converter by the piezo effect is modelled by voltage feedback \mathbf{v}_m . The modal amplitudes of both standing waves are represented by vector

$$\mathbf{w}^T = [w_{1s} \ w_{1c} \ w_{2s} \ w_{2c}] = [\mathbf{w}_1 \ \mathbf{w}_2]. \quad (4)$$

Under consideration of averaging for the vibrating stator the fundamental describing functions of modal force vector \mathbf{F}_d are of interest only, while for the rotor dynamics the dc-values of \bar{T}_M and F_{Rz} are important. Thus the averaged model of the contact interface is derived by using the extended describing function technique (Sanders, Noworolski, 1991). As indicated by the signal line for ω_s , the inverter's feeding frequency influences the dynamics of the converter and especially the stator causing modulation of the fundamental components.

Fig. 4 shows the comparison of a simulated and measured transient response of the ultrasonic drive reflecting the cartesian coordinates of the fundamental Fourier coefficients and the magnitude. As proven by this experimental results the model agrees sufficiently with the physical behaviour of the drive.

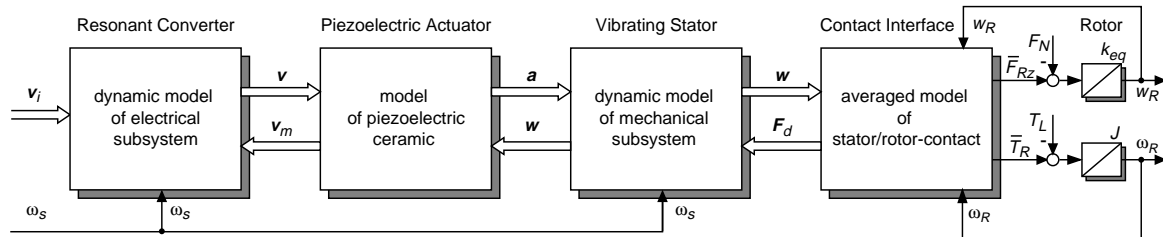


Figure 3: Simulation model of converter-fed ultrasonic motor with its functional modules.

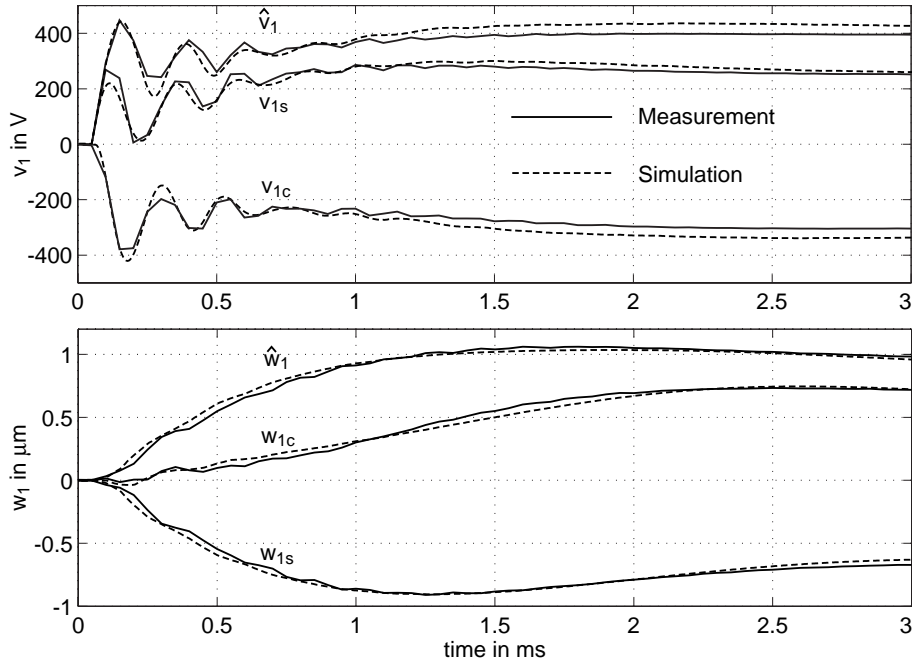


Figure 4: Transient response of the drive's ultrasonic oscillations (phase 1) to a step command of v_{inv1c} and v_{inv2s} from zero to 80 V at $t = 0$.

4. Bending Wave Control

4.1. Bending Wave Control scheme

The drive control scheme proposed in (Maas, Schulte et al., 1997) is based on the averaged model outlined before. The novel overall control scheme depicted in Fig. 5 shows a cascaded structure. Since two dynamic resonant systems characterize the oscillations of the USM-drive, it is obvious to control the motor by means of an inner voltage and an outer travelling bending wave control loop. Controlled quantities are the sine and cosine components of voltages v_1, v_2 and modal amplitudes w_1, w_2 measured by phase-sensitive demodulation circuits. Excellent drive performance is adjusted by the following systematical measures:

- The reference values v_i^* are passed to the vector modulation algorithm in order to calculate the regulating quantities $\beta_1, \beta_2, \varphi_1, \varphi_2$ of the two-phase inverter stage. A compensation of mechanical feedback v_m on the converter is introduced. The voltage control is denoted by the controllers $G_{Rel1,2}$.
- A compensation of couplings between mechanical vibrations is achieved by introducing the inverse model K_{pv}^{-1} of the piezoelectric actuator. An identical vector control scheme is applied for the bending wave control $G_{Rm1,2}$ as used for the voltage control. The command inputs of bending wave control are determined from the reference value of the speed control explained in detail in chapter 5.

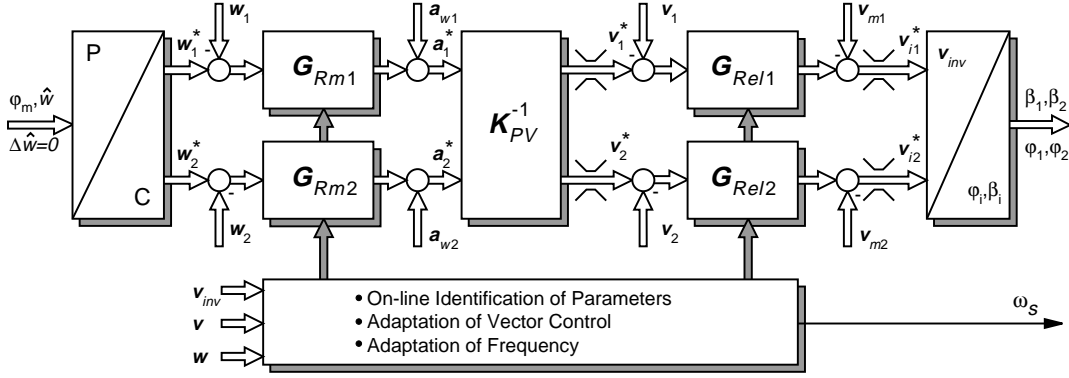


Figure 5: Voltage and bending wave vector control scheme of USM-drive.

- Remaining regulating quantity ω_s of the converter is adapted in such a way, that the vibration modes of the stator are excited at resonance. By this measure the optimal operating point of vibrator is found minimizing the voltage demand for excitation resulting in a loss reduction of converter and piezo ceramic.
- For obtaining a high dynamic response of the drive control in a wide operation range an on-line adaptation of control parameters is recommended due to nonlinear contact impacts and temperature influences. While temperature effects influence the electrical as well as mechanical subsystem, contact forces F_d have an impact on the mechanical system only. For on-line identification of slowly-varying plant parameters simple algorithms are used based on a quasi-stationary evaluation of the transfer matrices obtained from the averaged drive model, (Maas, Schulte et al., 1997). Impacts of fast parameter variations caused by contact forces are almost eliminated by an appropriate modulation of the frequency ω_s , see (Maas, Schulte, 1997).

4.2. Experimental results for bending wave controlled drive

As mentioned above the eigenvalue problem of mechanical vibrator is affected by nonlinear contact impacts. Two different types of contact forces acting on the stator are considered by $F_d = F_{dn} + F_{dt}$:

- Due to normal deflection of the stator's surface points normal contact forces occur, yielding the normal pressure distribution by which the feedback force F_{dn} causes a shift of the vibrator's eigenfrequency ω_m .
- By the horizontal deflection of surface points tangential contact forces result, producing the tangential pressure distribution for torque generation, which entails variations of the total damping δ_m by F_{dt} .

Eigenvalues $p_{(1,2)} = -\delta_m \pm j\omega_m$ depend strongly on the operating point, especially on the amplitude \hat{w} of the travelling bending wave.

By investigations of the drive under study it is turned out, that impacts of normal forces F_{dn} are dominant compared to the tangential forces F_{dt} . When designing the control normal contact forces cause stability problems, because the well known pull-out phenomenon of travelling wave USMs occurs observed by different authors (Furuya, et. al. 1992), (Senjyu, et. al.

1995). As illustrated in Fig. 6a this breakdown in frequency $f_{s,b}$ appears, when the feeding frequency ω_s is decreased below the resonance frequency ω_m . By increasing of ω_s until the actual resonance frequency is attained again ($f_{s,s}$), the rotor starts to revolve abruptly. Since a hysteresis loop is obtained when changing ω_s by this way, the effect is designated as hysteresis effect.

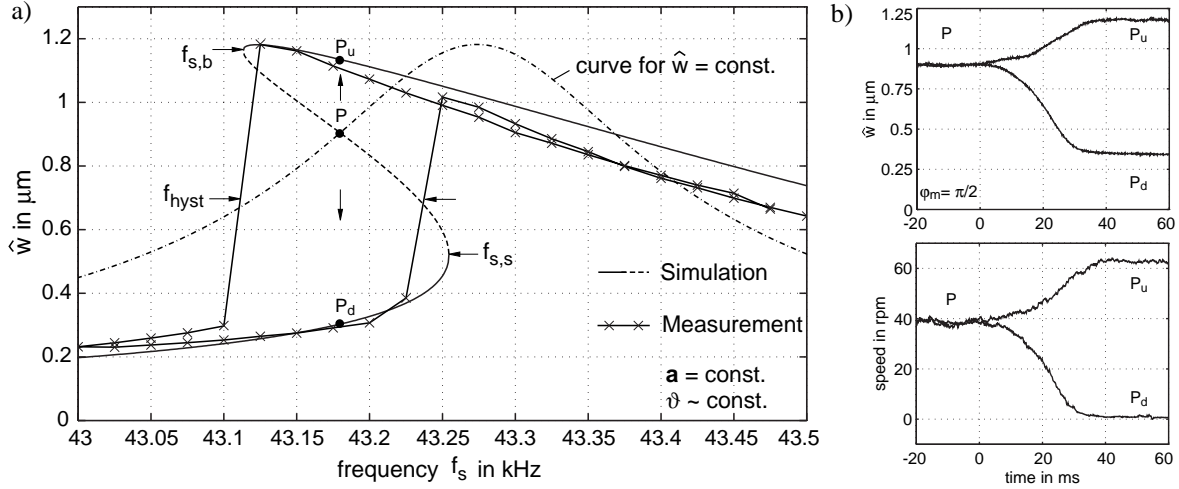


Figure 6: a) Nonlinear frequency characteristics of mechanical subsystem.
b) Instability caused by turn off of bending wave control at $t = 0$.

The reason is related to a degressive stiffness behaviour of the contact interface, since variations of the amplitude \hat{w} influence the width of contact area between stator and elastic contact material. For investigations of the nonlinear frequency characteristics of mechanical resonant tanks the gain is calculated by

$$|\hat{w}/a| = 1/\sqrt{(\omega_m^2(\hat{w}) - \omega_s^2)^2 + 4\delta_m^2\omega_s^2}, \quad (5)$$

using the contact model explained before. In Fig. 6a the calculated results are compared with measurements. While outside the hysteresis bandwidth single-valued curves are obtained, inside the bandwidth three solutions are calculated. Two of them are stable operating points, indicated also by the measured curve. It can be shown, that operating points marked by the dashed line characterize instabilities in case of frequency control.

Previously published control schemes use solely the frequency modulation for controlling the amplitude \hat{w} . It is obvious that the pull-out phenomenon can be avoided only, when a certain distance between resonance frequency ω_m and switching frequency ω_s is introduced (Senjyu et al., 1995) losing a wide range of the USMs performance. If the amplitude \hat{w} is controlled by an amplitude modulation instead of frequency modulation, operating points indicated as instabilities by the dashed line in Fig. 6a can be stabilized. Thus, the pull-out phenomenon can be avoided in general.

For verification the effect of stabilizing by the bending wave control, the reference value of the controlled amplitude is kept to $\hat{w}^* = 0,9\mu\text{m}$ and the difference between feeding frequency and eigenfrequency is chosen to $\Delta\omega_m = \omega_s - \omega_m = -2\pi \cdot 50\text{Hz}$, which characterize the

operating point P and the linear resonance curve for $\omega_m = \text{const}$ in Fig. 6a. At time instant $t=0\text{ms}$ the bending wave control is turned off as depicted in Fig. 6b. Due to small disturbances in practice the operating point of the voltage controlled drive shifts from instable point P to stable point P_u or P_d (high speed or stand still) depending on the effect of disturbances at $t \geq 0\text{ms}$. Operating points P_u , P_d belong to the hysteresis curve in Fig. 6a. As shown by these measurements an operation of USM-drives at the mechanical resonance and below this critical point is enabled when using a suitable drive control. For an operation at resonance, frequency ω_s is adapted to ω_m . The operation at the mechanical resonance furnishes the minimization of the feeding voltages; thus offers essential advantages for optimization of the drive's performance.

In order to prove the voltage decrease, measurements at different operating points within an appropriate range of the feeding frequency are performed and depicted in Fig. 7a, where \hat{w} is kept constant by the control. By changing the frequency difference $\Delta\omega_m$ between feeding frequency ω_s and eigenfrequency ω_m from $|2\pi \cdot 300\text{Hz}|$ to resonance $\Delta\omega_m = 0$ a remarkable reduction of the USMs voltage demand is achieved and therefore the converter losses and also the dielectrical losses are minimized. Previously published control schemes have applied a difference Δf_m of several hundred Hertz due to the pull-out phenomenon. Hence, a large potential for optimization was unexploited and a wide range of the USMs power performance is not utilized.

Finally, measured results of a transient response are depicted in Fig. 7b. A large step change of the amplitude \hat{w} from $\hat{w}^* = 0,5\mu\text{m}$ to $\hat{w}^* = 1\mu\text{m}$ ($|w_{s,c}| = 353\text{nm}$ to $|w_{s,c}| = 707\text{nm}$) at $t=0\text{ms}$ is performed. The controlled drive is loaded with $T_L = 0,5\text{Nm}$ by the dc-machine. The phase and frequency differences are kept constant to $\phi_m^* = 90^\circ$ and $\Delta\omega_m^* = 0$.

As indicated by the measurements the rise time of the modal amplitudes is only about 1 ms and the decoupling works sufficiently. The performed step change of \hat{w}^* represents a variation of the amplitude from its minimum (threshold for torque generation) to its maximum. A step-like command of such large amount is not applied by the speed control, which generates the reference values \hat{w}^* , ϕ_m^* . Hence, the measured responses satisfy requirements of an outer speed control. As indicated by the results of f_s , a large shift of eigenfrequencies ω_m of about $2\pi \cdot 400\text{Hz}$ is caused during the transient reaction of the amplitude \hat{w} . Corresponding impacts of the stator are well suppressed by the fast variation of the feeding frequency f_s .

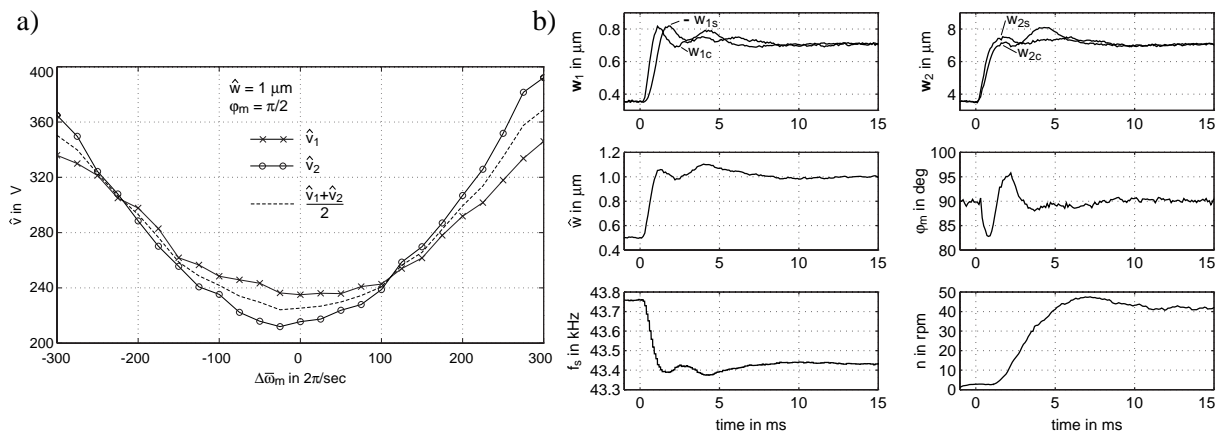


Figure 7: a) Voltage requirement versus $\Delta\bar{\omega}_m$ for constant modal amplitudes.

b) Large signal response of controlled drive for step change of \hat{w} .

5. Speed Controlled Drive

5.1. Inverse contact model by neural network

For optimization of the speed control (Maas, Grotstollen, 1996) the nonlinear torque generation of the USM must be compensated. While the torque of conventional electro-magnetic machines is depending almost linear on the current of the motor, the USMs torque T_M is nonlinear related to the amplitudes \hat{w}_1, \hat{w}_2 of both standing waves, the temporal phase shift φ_m between them and the rotor's speed ω_R , see (Maas, Ide et al., 1995). In order to compensate the nonlinear torque generation an inverse contact model is introduced between the speed controller and the bending wave control as depicted in Fig. 8. Due to extreme nonlinearities and interdependence of contact quantities a numerical approach by neural networks is predestinated for approximation of the inverse model. Since there are still some deviations between measured results and model predictions, sample points obtained by measurements are utilized for training the net with respect to a practical control design.

In (Maas, Ide et al., 1996) it is pointed out that an operation with a perfect-travelling wave is optimal for minimized losses caused by the friction interface. This conditions are obtained when the amplitudes \hat{w}_1, \hat{w}_2 are equal to a single value \hat{w} , representing the amplitude of the travelling bending wave, and when the phase φ_m is kept to $\pm 90^\circ$. Thus, variations of speed-torque curves should be performed by adjusting \hat{w} on one hand. But on the other hand the amplitude can not be decreased under a certain threshold \hat{w}_{min} due to tribological uncertainties caused mainly by slip-stick effects. Operating the drive in this inherent deadzone a non-perfect travelling wave is required by adjusting the phase φ_m . Thus, optimal torque utilization and minimized losses under consideration of the inherent amplitude threshold are obtained when:

- in any operation mode the amplitudes of both standing waves are equal, established by $\Delta\hat{w}^* = \hat{w}_1^* - \hat{w}_2^* = 0$,
- in the high-speed/high-torque region the USM is operated with a perfect travelling wave, obtained by adjusting $\hat{w}_{min} \leq \hat{w} \leq \hat{w}_{max}$ and $|\varphi_m| = 90^\circ$,
- in the low-speed/low-torque region the phase shift φ_m is used for the control and the amplitude is kept to $\hat{w} = \hat{w}_{min}$.

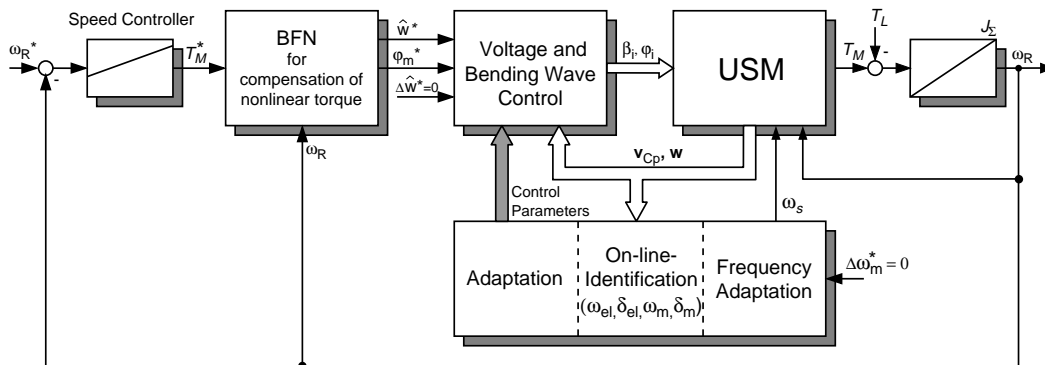


Figure 8: Overall scheme of speed controlled USM-drive using a neural network (BFN) for compensation of the nonlinear torque generation.

Considering the statements given above the measured curves of the USM under study results as depicted in Fig. 9a. While in the high-speed/high-torque range the amplitude is varied from $\hat{w}_{min} = 0,7\mu\text{m}$ to $\hat{w}_{max} = 1,2\mu\text{m}$ in steps of $0,1\mu\text{m}$ (solid lines), in the low-speed/low-torque region (dashed lines) the phase ϕ_m is adjusted to $[-50^\circ, -30^\circ, -15^\circ, 0^\circ, 15^\circ, 30^\circ, 50^\circ]$ controlling the amplitude above the threshold for an impeccable operation. Torque and speed of the USM are limited to $|T_M| = 3\text{Nm}$ and $|n| = 80\text{rpm}$ to prevent destruction. Since for servo applications a high dynamic USM-drive is aimed on, the whole operating range of speed-torque curves must be considered when designing the inverse contact model.

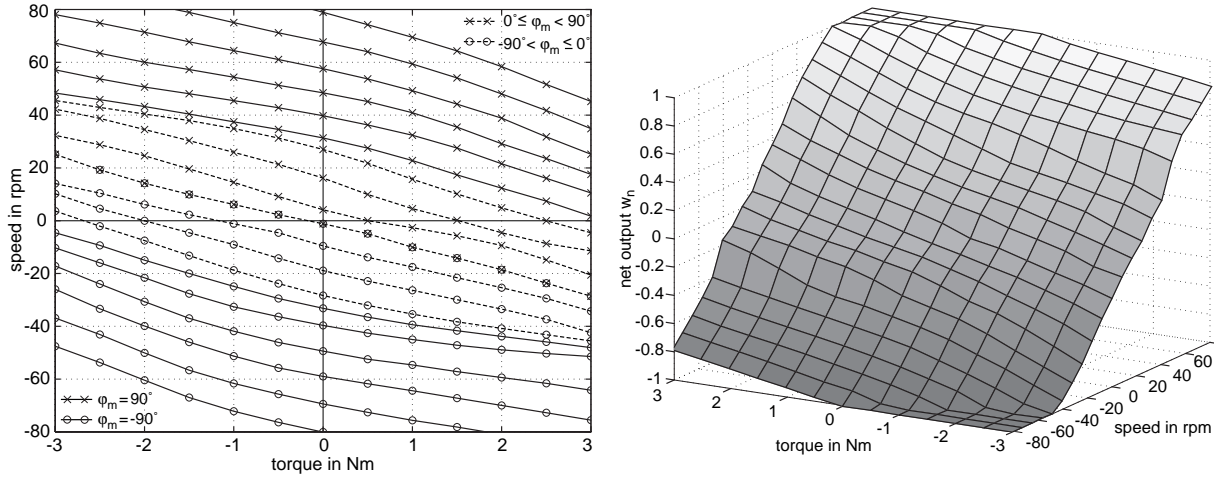


Figure 9: a) Measured speed-torque curves of the USM-drive under study.

b) Two-dimensional BFN for approximation of inverse contact model generating the reference values of bending wave control

In order to generate the reference values of bending wave control from desired torque T_M^* under consideration of actual speed ω_R , a two-dimensional basis function network (BFN with linear splines), applied for the inverse model, serves for interpolation between the samples of a look-up table. Measured values of Fig. 9a are utilized for off-line learning of the net. As mentioned before only one of the regulating quantities \hat{w}^* , ϕ_m^* is varied by the speed control. Thus, one BFN is sufficient for modelling the inverse characteristics when introducing a transformed regulating quantity w_n as outlined in (Maas, Schulte et al., July 1998). The BFN designed for the inverse model is depicted in Fig. 9b. A layer of 41 times 13 neurons for the speed and torque input is used, whereby the final fault Δw_n is less than 3%.

5.2. Speed Control

Since the reference values of the bending wave control are calculated from the desired torque value by the BFN under consideration of actual motor speed, the remaining nonlinearity of the motor's nonlinear torque generation is compensated and an almost linear relation between reference torque T_M^* and motor torque T_M is obtained. Thus, the command behaviour of the new actuator approaches that of conventional drives so that proven speed control schemes can be applied. For the mechanical example of a one mass system a linear PI speed controller is applied as illustrated in Fig. 8 by the overall scheme of the controlled USM-drive. The drive control is implemented on a DSP-controlled experimental set-up. Designing the PI-controller

the bending wave control is approximated by an appropriate first order lag. Besides this time constant, the time delay of the signal processing and the measuring system and the total inertia are taken into account.

In Fig. 10 the measured transient responses of the novel speed control are shown, while in Fig. 11 the operation is illustrated by the corresponding T_M^*-n trajectories within the operating range of Fig. 9a.

In case a) a command step response from the low-speed/low-torque region (operating point P1 with $n = 10\text{rpm}$ and $T_L = 0$) into the high-speed/high-torque region (operating point P2 with $n = 50\text{rpm}$ and $T_L = 0$) is performed. During the first time interval $0 \leq t \leq 3\text{ms}$ the reference value of the phase φ_m is increased by the BFN due to reference torque T_M^* , while the reference value of the amplitude is kept to $\hat{w}_{min} = 0,7\mu\text{m}$. When φ_m^* attains its maximum of 90° the speed is regulated by varying the reference value of the wave's amplitude \hat{w} , whereby the drive is operated finally with a perfect travelling wave. After a short rise time of about 10ms the desired speed is attained and the drive speed n settles smoothly to $n^* = 50\text{rpm}$ as expected by the design method for the speed control. Since the USM-drive is accelerated during this response, energy is stored in the total inertia of the system. Thus, the corresponding torque-speed trajectory for case a) passes almost the first (motory) quadrant in Fig. 11.

Case b) depicts the opposite operation mode: $P2 \rightarrow P1$. First, the reference value of the amplitude is decreased to its minimum $\hat{w}_{min} = 0,7\mu\text{m}$, while the phase φ_m^* is kept at 90° . Second, at $t = 4,5\text{ms}$ and $w_n = 0,4$ the speed is regulated finally by the reference value of φ_m .

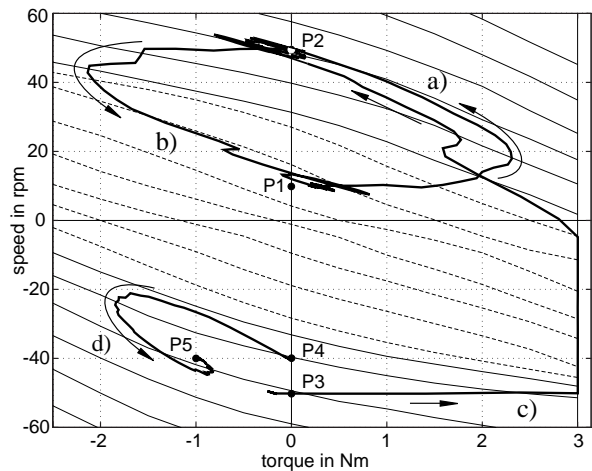
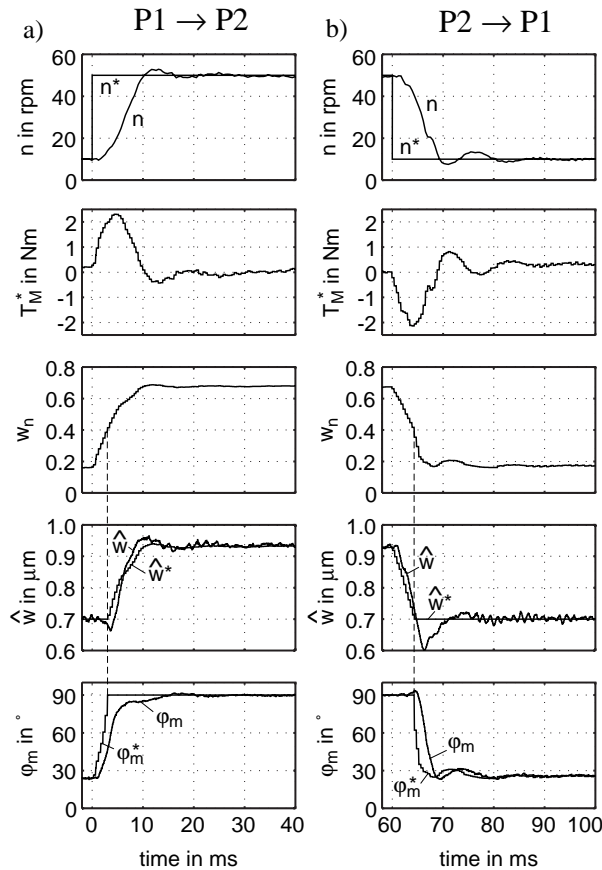


Figure 11: Corresponding torque-speed trajectories of Fig. 10.

Figure 10: Command and disturbance step responses of speed-controlled USM-drive with respect to operating points in Fig. 11.

Due to the sufficient compensation of nonlinear torque generation by the BFN the response time and overshoot is approximately identical when compared to case a). Since the drive is decelerated in case b), the corresponding torque-speed trajectory passes almost the second (non-motory) quadrant in Fig. 11.

In Fig. 11 the torque-speed trajectories of a speed reversal of the drive (c) and a step-like load change (d) are depicted additionally. The speed reversal is performed from $n^* = -50\text{rpm}$ to $n^* = 50\text{rpm}$ (P3 \rightarrow P2) and the reference torque reaches it's upper boundary. The step-like load change is performed from zero to $T_L=1\text{Nm}$ (P4 \rightarrow P5).

As indicated by the measurements, first the designed speed control ensures the optimized conditions as outlined by the speed-torque characteristics in Fig. 9 for high-speed/high-torque and low-speed/low-torque operation modes. Second the operation of the BFN, applied for compensation of nonlinearity, operates satisfactory as indicated by the expected transient responses of a linear speed controller.

6. Active Control Stick

Finally an Active Control Stick (ACS) realized by means of the controlled USM-drive should be noticed as an interesting kind of application. The main disadvantage of the conventional side stick in modern aircrafts is the absence of any feedback from the rudders. In order to realize an ACS (which allows active force feedback, Fig. 12) an actuator has to be introduced in the mechanical assembly of the stick. Minimizing the size and the weight of the whole device piezo motors seem to be predestinated for this application, because of their high power density and high torque at low rotational speed. In cooperation with industries (Daimler-Chrysler, SFIM Industries) a prototype ACS with a rotary travelling wave type USM was successfully realized using open loop torque control by the inverse contact model.

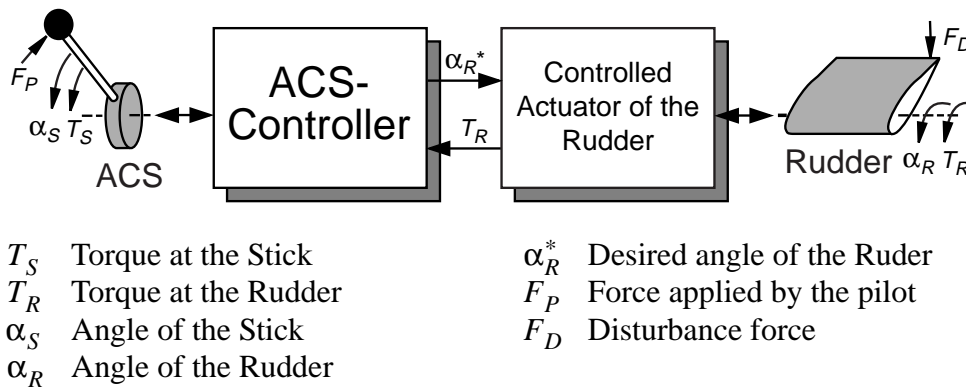


Figure 12: Principle of ACS.

7. Conclusion

In this paper an overall view on a model based control scheme for rotary travelling wave type USMs is given including the modelling steps. After a review of a simulation model for the overall drive system a two-phase vector control scheme for voltage and bending wave control is outlined. It is proved by experimental results, that on one hand an operation at the mechani-

cal resonance is feasible optimizing the drive's performance remarkably and on the other hand the high dynamic behaviour of the bending wave control satisfies requirements of a high performance speed control. The motor's nonlinear torque generation is compensated by a basis function network calculating the optimized reference values of underlaid bending wave control. Thus, a linear controller could be used for the speed control. The good performance of the speed controlled drive was proven by measurements, too.

The overall control scheme optimizes the total drive performance and suppresses the known disadvantages of travelling wave type ultrasonic motors. Thus, under consideration of typical features of this type of motors, the so equipped ultrasonic drive meets requirements for a wide field of applications.

8. Acknowledgement

The authors acknowledge gratefully the support of the Deutsche Forschungsgemeinschaft for financing this USM-project. Thanks belong to the Department Research and Technology - FT2/LA of Daimler-Chrysler in Frankfurt for supporting the institute with travelling wave type USMs.

9. References

Furuya S. et al. (1992):

Load-adaptive frequency tracking control implementation of two-phase resonant inverter for ultrasonic motor. IEEE Trans. on Power Electronics, Vol. 7, No. 3, July 1992, pp. 542-550.

Sashida, T.; Kenjo T. (1993):

An introduction to ultrasonic motors.
Clarendon Press - Oxford (1993)

Hagood, N.; McFarland, J. (1995):

Modelling of a Piezoelectric Rotary Ultrasonic Motor.
IEEE Transactions on Ultrasonic, Ferroelectrics, and Frequency Control, VOL. 42, NO. 2, March 1995

Flynn, A. M. (1993):

Torque production in ultrasonic motors.
Private communication, MIT Artificial Intelligence Lab., Dec. 1993

Senjyu, T. et al. (1995):

Quick and Precise Position Control of Ultrasonic Motors with Two Control Inputs.
IEEE Power Electronic Specialists Conf. 1995 (PESC'95), Atlanta, pp. 415-420, June 1995.

Sanders, S. R.; Noworolski, J. M.; Lui, X.Z.; Verghese, G. C. (1991):

Generalized Averaging Method for Power Conversion Circuits.
IEEE Transaction on Power Electronics, Vol. 6, No. 2, pp. 251-258, 1991.

Maas, J.; Fröhleke, N.; Krafka, P.; Grotstollen, H. (1995):

Prototype Drive and Modulation Concept for DSP-Controlled Ultrasonic Motors powered by Resonant Converters.
European Power Electronics Conf. 1995 (EPE'95), Sevilla (Spain), pp. 1777-1782, Sept. 1995

Maas, J.; Ide, P.; Grotstollen H. (1995):

Simulation Model for Ultrasonic Motors powered by Resonant Converters.
IEEE Ind. Applic. Soc. Conf. 1995 (IAS'95), Orlando, Vol. 1, pp. 111-120, Oct. 1995

Maas, J.; Ide, P.; Grotstollen H. (1996):

Characteristics of Inverter-Fed Ultrasonic Motors – Optimization of Stator/Rotor-Interface.
5th Int. Conference on New Actuators - ACTUATOR'96, Bremen, pp. 241-244, 1996

Maas, J.; Grotstollen H. (1997):

Averaging Model for Inverter-Fed Ultrasonic Motors.
IEEE PESC '97, St. Louis, Vol. 1, pp. 740-746, 1997

Maas, J.; Schulte, T.; Grotstollen H. (1997):

Optimized Drive Control for Inverter-Fed Ultrasonic Motors.
IEEE IAS '97, New Orleans, Vol. 1, pp. 690-698, 1997

Maas, J.; Schulte, T.; Grotstollen H. (June 1998):

High Performance Speed Control for Inverter-Fed Ultrasonic Motors by a Neural Network.
ACTUATOR '98, Bremen, pp. 260-263, June 1998

Maas, J.; Schulte, T.; Grotstollen H. (July 1998):

Controlled Ultrasonic Motor for Servo-Drive Applications.
4th European Conf. on Smart Structures and Materials and 2nd International Conf. on Micromechanics, Intelligent Materials and Robotics (MIMR '98), Harrogate (UK), pp. 701-708, July 1998.